

Superconductivity and non-metallicity induced by doping the topological insulators Bi_2Se_3 and Bi_2Te_3

Y. S. Hor¹, J. G. Checkelsky², D. Qu², N. P. Ong², and R. J. Cava¹

¹Department of Chemistry, Princeton University, New Jersey 08544, USA

²Department of Physics, Princeton University, New Jersey 08544, USA

Abstract

We show that by Ca-doping the Bi_2Se_3 topological insulator, the Fermi level can be fine tuned to fall inside the band gap and therefore suppress the bulk conductivity. Non-metallic Bi_2Se_3 crystals are obtained. On the other hand, the Bi_2Se_3 topological insulator can also be induced to become a bulk superconductor, with $T_c \sim 3.8$ K, by copper intercalation in the van der Waals gaps between the Bi_2Se_3 layers. Likewise, an as-grown crystal of metallic Bi_2Te_3 can be turned into a non-metallic crystal by slight variation of the Te content. The Bi_2Te_3 topological insulator shows small amounts of superconductivity with $T_c \sim 5.5$ K when reacted with Pd to form materials of the type $\text{Pd}_x\text{Bi}_2\text{Te}_3$.

Introduction

A novel kind of three-dimensional insulator called topological insulators, which have a bulk band gap but non-trivial topological surface states has been introduced [1–5]. The surface states of these topological insulators show Dirac-like behavior with the spin polarization locked perpendicular to the electron momentum by the effect of strong spin-orbit interaction. Recently, a new class of topological insulators, Bi_2Se_3 and Bi_2Te_3 , previously known to be a good thermoelectric materials [6], has been discovered [7,8,9,10]. The surface states of these materials have been observed by angle-resolved photoemission spectroscopy (ARPES) [7,8,9] and scanning tunneling microscopy (STM) [11,12], but are still considered a challenging problem for electronic transport measurements due to their dominant bulk conductance. Here we show that, by proper chemical doping, we can suppress bulk conduction in Bi_2Se_3 and Bi_2Te_3 , which is necessary for the detection of the surface currents. The electronic transport detection of the surface Dirac state is important for the study of Majorana fermionic physics [13]. As proposed in the reference 13, finding the Majorana fermion requires an interfacing of a topological insulator with a superconductor. We further show that by proper intercalation of transition metal elements, superconductivity can be induced in the Bi_2Se_3 and Bi_2Te_3 topological insulators.

Experimental

The tetradymite Bi_2Se_3 and Bi_2Te_3 single crystals were grown by a modified Bridgman method, melting stoichiometric mixtures of high purity elements of Bi (99.999 %), Se (99.999 %) or Te (99.999 %) at 800 °C for 16 hours and then slow cooling to 550 °C in sealed vacuum quartz tubes. The crystals were then annealed at 550 °C for three

days. Since Ca can react with quartz, a proper procedure is required - the two step method described in ref. 14 was used to grow $\text{Bi}_{2-x}\text{Ca}_x\text{Se}_3$ crystals. To obtain non-metallic Bi_2Te_3 , the as-grown stoichiometric crystal was annealed under Te vapor at 410 °C for a period of one week with ~0.5 g Te in a sealed quartz tube of volume ~8 cm³. Single crystals of $\text{Cu}_y\text{Bi}_2\text{Se}_3$ were grown by melting stoichiometric mixtures of high purity elements Bi (99.999 %), Cu (99.99 %) and Se (99.999 %) at 850 °C overnight in sealed evacuated quartz tubes. The crystal growth took place via slow cooling from 850 to 620 °C and then quenching in cold water in order to optimize the quality of the Cu-intercalated Bi_2Se_3 crystals. The cleaved silvery surfaces of these crystals turn golden after one day exposure to air, suggesting that exposure to air should be kept to a minimum. $\text{Pd}_z\text{Bi}_2\text{Te}_3$ crystals can be grown by the same method; high purity Pd (99.99 %) was used.

All the grown crystals were cleaved very easily along the basal plane, leaving a silvery shining mirror like surface, and were cut into approximately $1.0 \times 1.0 \times 6.0 \text{ mm}^3$ rectangular bar samples for electronic transport measurement. The rhombohedral crystal structure of all the as-grown and annealed crystals was confirmed by x-ray powder diffraction (XRD) using a Bruker D8 diffractometer with Cu K α radiation and a graphite diffracted beam monochromator. Resistivity and magnetoresistance measurements were performed in a Quantum Design physical property measurement system (PPMS) between 1.8 and 300 K, where the standard four-probe technique with silver paste cured at room temperature was used for the electrical transport contacts on a freshly cleaved surface. The measurements were conducted with the applied magnetic field along the *c*-axis with the electric-currents parallel to the basal plane of the crystals. The potential contacts were made on the cleavage surface. Hall Effect measurements to determine carrier

concentrations were performed in a home-built apparatus. AC magnetization measurement was performed in the PPMS with a magnetic field of amplitude 5 Oe.

Results and Discussions

Bi₂Se₃

XRD results confirm the rhombohedral crystal structure of Bi₂Se₃, which consists of Bi and Se hexagonal planes stacked along the [001] crystallographic direction or *c*-axis (hexagonal setting), with the atomic order, Se(1)-Bi-Se(2)-Bi-Se(1), where (1) and (2) refer to different lattice positions [15]. The unit cell consists of three of these units stacked on top of each other with weak van-der-Waals bonds between Se(1)-Se(1) layers, making the (001) plane the natural cleavage plane. In reality, an as-grown Bi₂Se₃ crystal tends to have Se vacancies, giving rise to an excess of electrons. In reference 14, STM measurements show that Se vacancy defects are present in Bi₂Se₃ crystals, giving rise to an excess of electrons in the system which bring the Fermi level into the conduction band. The spectra of Bi₂Se₃ obtained from scanning tunneling spectroscopy (*dI/dV*) were *n*-type, as expected, due to the presence of Se vacancies, and was confirmed by ARPES as is schematically sketched in Fig. 1(a). Thus the STM data support the defect chemistry model described above for the Ca-doped Bi₂Se₃, with the added observation that the concentration of defects in general is lower in the Ca-doped samples than for native Bi₂Se₃ [14].

The temperature-dependent resistivities in the *ab* plane for undoped Bi₂Se₃ and Bi_{2-x}Ca_xSe₃ crystals with *x* = 0.005 and 0.0025 are shown in Fig. 1(b). Both Bi₂Se₃ and Bi_{1.995}Ca_{0.005}Se₃ show the weakly metallic resistivities commonly seen in high carrier concentration small band gap semiconductors, with resistivities in the 0.3 to 1.5 mΩ-cm

range at temperatures near 10 K. The lightly doped $x = 0.005$ material is p -type with a carrier concentration at $T = 1.5$ K determined by Hall effect measurements as shown in the inset of Fig. 1(b) to be approximately $1 \times 10^{19} \text{ cm}^{-3}$, whereas for the n -type Bi_2Se_3 , the carrier concentration is $8 \times 10^{17} \text{ cm}^{-3}$. For the n -type Bi_2Se_3 crystal, the valence band and a small pocket of the conduction band near the Γ point are clearly observed below E_F in ARPES data [14] as shown in the left plot of Fig. 1(a). $\text{Bi}_{1.995}\text{Ca}_{0.005}\text{Se}_3$ has the E_F in the valence band (Fig. 1(a) right) showing a p -type carrier which is consistent with the Hall effect measurement as shown in the inset of Fig. 1(b). This E_F shift indicates that the Ca doped crystal is hole doped relative to the n -type Bi_2Se_3 crystal. In the p -type doped samples, the Fermi level is below the energy of the Dirac point. By fine tuning with 0.125 % Ca doping in Bi_2Se_3 , we achieve the goal of obtaining a non-metallic Bi_2Se_3 topological insulator, where its resistivity increases to a very large value of $\sim 70 \text{ m}\Omega\text{cm}$ as temperature decreases to 100 K. This is consistent with the ARPES data [16] as sketched in the center of Fig. 1(a) that the E_F is dramatically lowered to lie very close to the Dirac point, and therefore of interest in fundamental and applied studies of the topological surface states [17].

Cu_xBi₂Se₃

Single crystals of Cu-intercalated Bi_2Se_3 , $\text{Cu}_y\text{Bi}_2\text{Se}_3$ within the composition range $0.10 < y < 0.15$ are reproducibly superconducting whereas single crystals of Cu-substituted Bi_2Se_3 , $\text{Bi}_{2-y}\text{Cu}_y\text{Se}_3$ prepared for $y = 0$ to 0.15 are never superconducting. For all $\text{Cu}_y\text{Bi}_2\text{Se}_3$ crystals, we observe from XRD that a subtle increase in the c -axis lattice parameter, from $c \sim 28.67 \text{ \AA}$ for Bi_2Se_3 to $c \sim 28.73 \text{ \AA}$ for $\text{Cu}_{0.12}\text{Bi}_2\text{Se}_3$ [18]. By analogy to the similar behavior in observed related layered Cu_xTiSe_2 [19], we infer that the

intercalated Cu in the van der Waals gap partially occupies the octahedrally coordinated $3b$ $(0, 0, \frac{1}{2})$ sites in the $R\bar{3}m$ space group [18]. In reference 18, STM has confirmed that the Cu is indeed intercalated in between Bi_2Se_3 layers and also showed that there is no Cu cluster formation within the van der Waals layers below the exposed surface.

Figure 2(a) shows the temperature dependence of the resistivity of the Bi_2Se_3 , $\text{Cu}_{0.1}\text{Bi}_2\text{Se}_3$, $\text{Cu}_{0.12}\text{Bi}_2\text{Se}_3$, and $\text{Cu}_{0.15}\text{Bi}_2\text{Se}_3$ single crystals, measured in the ab plane. The resistivities of the crystals show weakly metallic in the whole range of temperature except for the Bi_2Se_3 that has slight increase in its resistivity at temperatures below 20 K. The $\text{Cu}_y\text{Bi}_2\text{Se}_3$ superconducting crystals have about one order magnitude lower resistivity than Bi_2Se_3 which is consistent with the Hall effect measurement [18]. The Hall effect measurements indicated that these superconducting crystals are n -type, with a temperature independent carrier density of approximately $\sim 2 \times 10^{20} \text{ cm}^{-3}$. This carrier concentration is one order of magnitude higher than is found in native Bi_2Se_3 [20,21], and two orders of magnitude higher than is found for crystals with chemical potentials tuned by Ca doping [14,17]. The superconducting transition for $\text{Cu}_{0.12}\text{Bi}_2\text{Se}_3$, which is expanded in the inset of Fig. 2(a), occurs at ~ 3.8 K. The resistivity does not drop to zero below T_c however, indicating that there is not a continuous superconducting path in the crystal. We attribute this to the sensitivity of the superconducting phase to processing and stoichiometry as discussed in reference 18.

Zero field cooled (ZFC) ac magnetization of the single crystals of $\text{Cu}_y\text{Bi}_2\text{Se}_3$ for $y = 0.1, 0.12, \text{ and } 0.15$ is shown in Fig. 2(b). Independent of y , the superconducting transition temperature is approximately 3.8 K, but the signal amplitude is increased with the increase of y , giving the highest amplitude as $\sim 0.025 \text{ emug}^{-1}$ at 1.8 K for $y = 0.15$.

This amplitude is about 20 % of that expected for full diamagnetism, but that estimate represents a lower limit because temperatures substantially below the transition were not accessible in our apparatus and the transition is not complete at the temperature where the field is applied for the ZFC measurement. The inset of Fig. 2(b) shows field dependence of the transverse resistivity, ρ_{xx} for $\text{Cu}_{0.12}\text{Bi}_2\text{Se}_3$ crystal with the magnetic field applied parallel to the c -axis. The upper critical field H_{c2} can be determined, confirming that the system is a type II superconductor.

Bi₂Te₃

Bi_2Te_3 has identical structure to Bi_2Se_3 . Similar to the Bi_2Se_3 case, as-grown Bi_2Te_3 always shows metallic behavior. In contrast to Bi_2Se_3 , stoichiometric Bi_2Te_3 crystals tend to have anti-structure defects in which Bi atoms go on a Te site [22], resulting p -type material with hole concentration near 10^{19} cm^{-3} . Due to the complexity of the Bi-Te thermodynamic phase diagram [23], even the most perfect crystals have a relatively large number of antisite defects. This in fact leads to variations in the electronic properties of as-grown crystals. Unlike Bi_2Se_3 , where acceptors such as Ca can be introduced into the system to compensate the defect caused by Se vacancies, the antisite defect in Bi_2Te_3 can be hardly resolved. However, by annealing Bi_2Te_3 crystals in closed systems with polycrystalline buffer material just below the melting point, the defect concentrations can be varied [23]. Here, we employ lower temperature annealing of initially p -type crystals in Te vapor to obtain non-metallic samples. Fine tuning with this technique to bring the E_F into the bulk gap is possible in the Bi_2Te_3 system.

The electronic properties of Bi_2Te_3 can be changed by slight variation of the Te content in the crystal. Figure 3 shows the transport property as a function of temperature

for *S1*, *S2*, *S3*, and *S4* samples. Most of the as-grown crystals, just like *S1*, exhibit metallic behavior over the whole range of temperatures. However, non-metallic behavior can be achieved through a slight increase of the Te content in the crystal by Te-vapor annealing. Non-metallic samples, *S2* and *S3* show a very different temperature dependence of resistivity. For *S3*, it behaves like a metal on decreasing temperature from 300 to 180 K, where a minimum is reached. As temperature decreases, the resistivity increases, reaching the maximum of 2.7 mΩcm at $T \sim 100$ K, where it then reverts to metallic behavior down to ~ 20 K and finally rises slightly below 20 K. The upper inset of Fig. 3 shows the sketch of the surface state dispersion [9] near the Γ point where the dash lines indicate the suggested Fermi levels of the *S1*, *S2*, and *S3* samples.

The lower panel of Fig. 3 shows the influence of magnetic field on the temperature dependent transport properties of the *S4* crystal, which is found to exhibit a significant magneto response in the entire temperature range below 300 K. In a 9 T field, it has magnetoresistance (defined as $MR = \frac{\rho_H - \rho_0}{\rho_0} \times 100\%$ where ρ_H and ρ_0 are the resistivities at H and 0 applied magnetic fields respectively), $MR \sim 1400\%$ at 2 K and $\sim 30\%$ at room temperature. The temperature dependent resistivity becomes more insulating in 9 T applied field. The lower inset in Fig.3 shows the temperature dependent Hall densities of the *S4* crystal. Hall resistivity measurements performed at magnetic fields close to 9 T, yield the Hall densities of the *S4* sample as $1.7 \times 10^{19} \text{ cm}^{-3}$ at room temperature and $9 \times 10^{18} \text{ cm}^{-3}$ at below 20 K.

Pd_zBi₂Te₃

Superconductivity can be found in Pd-added Bi_2Te_3 , with a superconducting transition at about 5.5 K. The as-grown $\text{Pd}_z\text{Bi}_2\text{Te}_3$ crystals for $z = 0.1, 0.15, 0.3, 0.5,$ and 1 have an identical structure to Bi_2Te_3 crystal but with a slight change in c parameter. XRD shows that there are minor impurity phases, such as PdTe_2 , BiPdTe , and $\text{Pd}_{72}\text{Bi}_{19}\text{Te}_9$ present in some samples, but none of them shows a superconducting transition at 5.5 K. However, BiPdTe , which is a known superconductor with the reported T_c as 1.2 K [24], shows a superconducting transition with the onset $T_c \sim 2$ K in our magnetic susceptibility and resistivity measurements.

In Figure 4, we show the ZFC ac magnetic susceptibility data for the Pd-added Bi_2Te_3 crystals. $\text{Pd}_z\text{Bi}_2\text{Te}_3$ crystals with $z = 0.15, 0.3, 0.5,$ and 1 show the superconducting transition at about 5.5 K, whereas $\text{Bi}_{2-x}\text{Pd}_x\text{Te}_3$ and other impurity phases do not. Besides, there is a 2 K superconducting transition present in some crystals, which is attributed to the presence of the BiPdTe phase. These transitions are consistently observed in the resistivity data, which is plotted in the inset of Figure 4 as the normalized resistivity with respect to the 10 K resistivity, ρ/ρ_{10K} for $z = 0.3, 0.5,$ and 1, with the measured 10 K resistivities being 96, 92, and 146 $\mu\Omega\text{cm}$ respectively. Though the magnetic susceptibility plots of Pd-added Bi_2Te_3 superconductors have a broader transition below 5.5 K, the resistivity plots have a sharp transition. However, the resistivities do not drop to zero below the transition, which could be due to the same situation as present in the $\text{Cu}_y\text{Bi}_2\text{Se}_3$ superconductors. The superconducting phase fraction is small in $\text{Pd}_x\text{Bi}_2\text{Te}_3$, which is estimated to be about 1 % of the superconducting volume fraction, based on the ac magnetic susceptibility signal at 2 K for $z = 1$ compound.

We suggest that the data show that Pd intercalated Bi_2Te_3 gives rise to superconductivity, just like Pd intercalated TiSe_2 [25] shows a superconductor with $T_c \sim 2$ K. The small fraction of superconducting volume in the $\text{Pd}_z\text{Bi}_2\text{Te}_3$ crystals could be due to the difficulty in having the Pd intercalated in between the Bi_2Te_3 layers. Besides, the antisite defects occurring in Bi_2Te_3 may prevent the intercalation. Whether this is true or not, more work is needed in the future, such as STM and TEM measurements, to confirm this argument.

Conclusion

We have shown that one can tune the electronic properties of Bi_2X_3 topological insulators by doping effects. Through consideration of the defect chemistry of Bi_2Se_3 , we have identified Ca as a dopant that when present in small percent quantities results in the formation of *p*-type charge carriers and further decreases its bulk conductivity. Ca-doping to $\text{Bi}_{1.9975}\text{Ca}_{0.0025}\text{Se}_3$ allows the Fermi level to be tuned to the Dirac point, making this material of substantial interest for the physics and technological studies proposed for topological insulators. *p*-type Bi_2Te_3 can also be tuned into an insulator by annealing the crystal at Te vapor at a low temperature. Use of this simple annealing method facilitates the tuning of the carrier concentrations in Bi_2Te_3 crystals to allow for study of surface transport associated with the topological surface states. Besides, these topological insulators can be doped to display superconductivity at accessible temperatures. We have shown that the topological insulator Bi_2Se_3 (Bi_2Te_3) can be made into a superconductor by Cu (Pd) intercalation between the Bi_2Se_3 (Bi_2Te_3) layers. This implies that Cooper pairing in the topological insulators is possible. Because of their structural compatibility, devices with interfaces between a Bi_2Se_3 (Bi_2Te_3) topological insulator and $\text{Cu}_y\text{Bi}_2\text{Se}_3$

(Pd₂Bi₂Te₃) superconductor can be fabricated for investigating novel concepts in physics based on topological surface states.

Acknowledgements

This work was supported by the NSF MRSEC program, grant DMR-0819860.

References

- [1] B. A. Bernevig, T. Hughes, and S. C. Zhang, *Science* 314 (2006) 1757.
- [2] B. A. Bernevig and S. C. Zhang, *Phys. Rev. Lett.* 96 (2006) 106802.
- [3] L. Fu, C. L. Kane, and E. J. Mele, *Phys. Rev. Lett.* 98 (2007) 106803.
- [4] J. E. Moore, and L. Balents, *Phys. Rev. B* 75 (2007) 121306(R).
- [5] L. Fu and C. L. Kane, *Phys. Rev. B* 76 (2007) 045302.
- [6] H. Scherrer and S. Scherrer, *CRC Handbook of Thermoelectrics*, edited by D. M. Rowe (Chemical Rubber, Boca Raton, FL, 1995), pp. 211-237..
- [7] Y. Xia, D. Qian, D. Hsieh, L. Wray, A. Pal, A. Bansil, D. Grauer, Y. S. Hor, R. J. Cava, and M. Z. Hasan, *Nature Phys.* 5 (2009) 398.
- [8] D. Hsieh, Y. Xia, D. Qian, L. Wray, F. Meier, J. H. Dil, J. Osterwalder, L. Patthey, A. V. Federov, H. Lin, A. Bansil, D. Grauer, Y. S. Hor, R. J. Cava, and M. Z. Hasan, *Phys. Rev. Lett.* 103 (2009) 146401.
- [9] Y. L. Chen, J. G. Analytis, J.-H. Chu, Z. K. Liu, S.-K. Mo, X. L. Qi, H. J. Zhang, D. H. Lu, X. Dai, Z. Fang, S. C. Zhang, I. R. Fisher, Z. Hussain, and Z.-X. Shen, *Science* 325 (2009) 178.
- [10] H. Zhang, C.-X. Liu, X.-L. Qi, X. Dai, Z. Fang, and S.-C. Zhang, *Nature Physics* 5 (2009) 438.
- [11] T. Zhang, P. Cheng, X. Chen, J.-F. Jia, X. Ma, K. He, L. Wang, H. Zhang, X. Dai, Z. Fang, X. Xie, and Q.-K. Xue, *Phys. Rev. Lett.* 103 (2009) 266803.
- [12] Z. Alpichshev, J. G. Analytis, J.-H. Chu, I. R. Fisher, Y. L. Chen, Z. X. Shen, A. Fang, and A. Kapitulnik, *Phys. Rev. Lett.* 104 (2010) 016401.
- [13] L. Fu and C. L. Kane, *Phys. Rev. Lett.* 100 (2008) 096407.

- [14] Y. S. Hor, A. Richardella, P. Roushan, Y. Xia, J. G. Checkelsky, A. Yazdani, M. Z. Hasan, N. P. Ong, and R. J. Cava, *Phys. Rev. B* **79** (2009) 195208.
- [15] S. K. Mishray, S. Satpathy, and O. Jepsen, *J. Phys.: Condens. Matter* **9** (1997) 461.
- [16] D. Hsieh, Y. Xia, D. Qian, L. Wray, J. H. Dil, F. Meier, J. Osterwalder, L. Patthey, J. G. Checkelsky, N. P. Ong, A. V. Fedorov, H. Lin, A. Bansil, D. Grauer, Y. S. Hor, R. J. Cava, and M. Z. Hasan, *Nature (London)* **460** (2009) 1101.
- [17] J. G. Checkelsky, Y. S. Hor, M.-H. Liu, D.-X. Qu, R. J. Cava, and N. P. Ong, *Phys. Rev. Lett.* **103** (2009) 246601.
- [18] Y. S. Hor, A. J. Williams, J. G. Checkelsky, P. Roushan, J. Seo, Q. Xu, H. W. Zandbergen, A. Yazdani, N. P. Ong, and R. J. Cava, *Phys. Rev. Lett.* **104**, 057001 (2010).
- [19] E. Morosan, H.W. Zandbergen, B.S. Dennis, J.W.G. Bos, Y. Onose, T. Klimczuk, A.P. Ramirez, N.P. Ong, and R.J. Cava, *Nature Phys.* **2** (2006) 544.
- [20] L. P. Jr Caywood and G. R. Miller, *Phys. Rev. B* **2** (1970) 3209.
- [21] A. Vaško, L. Tichý, J. Horák, and J. Weissenstein, *Appl. Phys.* **5** (1974) 217.
- [22] G. R. Miller and C.-Y. Li, *J. Phys. Chem. Sol.* **26** (1965) 173.
- [23] J. P. Fleurial, L. Gailliard, R. Triboulet, H. Scherrer, and S. Scherrer, *J. Phys. Chem. Solids* **49** (1988) 1237.
- [24] F. Hulliger and J. Muller, *J. Phys. Lett.* **5** (1963) 226; F. Hulliger, *Nature* **198** (1963) 382.
- [25] E. Morosan, K. E. Wagner, Liang L. Zhao, Y. Hor, A. J. Williams, J. Tao, Y. Zhu, and R. J. Cava, *Phys. Rev. B* **81**, 094524 (2010).

Figure Captions

Fig. 1. (a) Tuning the bulk Fermi level, E_F in Ca-doped Bi_2Se_3 . ARPES images in ref. [Hsieh nature] showed that the E_F lies in the bulk conduction (BC) band for Bi_2Se_3 (left), inside the bulk band gap for $\text{Bi}_{1.9975}\text{Ca}_{0.0025}\text{Se}_3$ (center), and in the bulk valence band (BV) for $\text{Bi}_{1.995}\text{Ca}_{0.005}\text{Se}_3$ (right). (b) Temperature dependent resistivity in the ab plane of Bi_2Se_3 , $\text{Bi}_{1.9975}\text{Ca}_{0.0025}\text{Se}_3$, and $\text{Bi}_{1.995}\text{Ca}_{0.005}\text{Se}_3$ crystals. The stoichiometric Bi_2Se_3 crystal is n -type and the Ca-doped materials are all p -type. The inset shows the Hall effect data at $T=1.5$ K [14] employed to determine the carrier concentrations for a Bi_2Se_3 crystal with an electron carrier concentration of $8 \times 10^{17} \text{ cm}^{-3}$ and $\text{Bi}_{1.995}\text{Ca}_{0.005}\text{Se}_3$ crystal with a hole carrier concentration of $1 \times 10^{19} \text{ cm}^{-3}$.

Fig. 2. (a) Temperature dependent resistivity of Bi_2Se_3 , $\text{Cu}_{0.1}\text{Bi}_2\text{Se}_3$, $\text{Cu}_{0.12}\text{Bi}_2\text{Se}_3$, and $\text{Cu}_{0.15}\text{Bi}_2\text{Se}_3$ single crystals with applied current in the ab -plane. The inset shows the resistivity behavior of a $\text{Cu}_{0.12}\text{Bi}_2\text{Se}_3$ crystal for $1 < T < 6$ K. (b) The temperature dependent magnetization of $\text{Cu}_{0.1}\text{Bi}_2\text{Se}_3$, $\text{Cu}_{0.12}\text{Bi}_2\text{Se}_3$, and $\text{Cu}_{0.15}\text{Bi}_2\text{Se}_3$ single crystals shows a superconducting transition $T_c \sim 3.8$ K in zero field cooled (ZFC) ac susceptibility measurements. The inset shows field dependence of the transverse resistivity, ρ_{xx} at several temperatures below 5 K for a single crystal of $\text{Cu}_{0.12}\text{Bi}_2\text{Se}_3$ with the magnetic field applied parallel to the c -axis.

Fig. 3. The upper panel shows the resistivities as a function of temperature of the as-grown and annealed Bi_2Te_3 crystals labeled as $S1$, $S2$ and $S3$. The inset in the upper panel shows the sketch of the surface state dispersion [9] near the Γ point where the dash lines indicate the suggested Fermi levels of $S1$, $S2$, and $S3$ samples. The lower panel shows the temperature dependent resistivity of $S4$ Bi_2Te_3 crystal in zero and 9 T applied magnetic

fields. Hall density n_H of *S4* Bi₂Te₃ crystal is plotted in the lower inset for the whole range of temperatures.

Fig. 4. Temperature-dependent ac magnetic susceptibilities for Pd_{*z*}Bi₂Te₃ crystals, with $z = 0.15, 0.3, 0.5$ and 1 . No superconductivity is found in Bi_{2-*z*}Pd_{*z*}Te₃, PdTe₂, and Pd₇₂Bi₁₉Te₉. The inset depicts the low-temperature resistivity data for Pd_{*z*}Bi₂Te₃, showing the superconducting transition $T_c \sim 5.5$ K for $z = 0.3, 0.5$ and 1 .

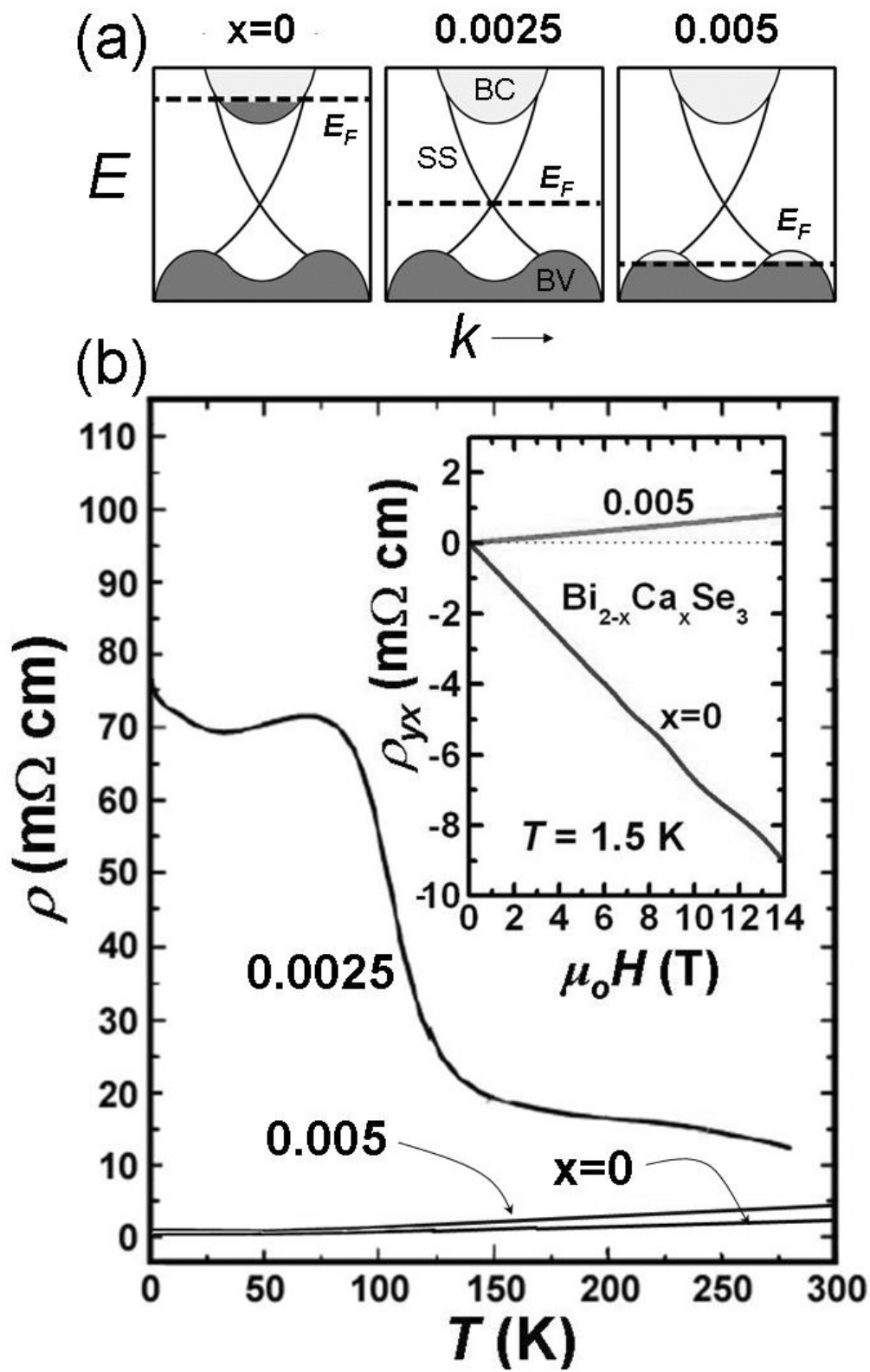


Figure 1

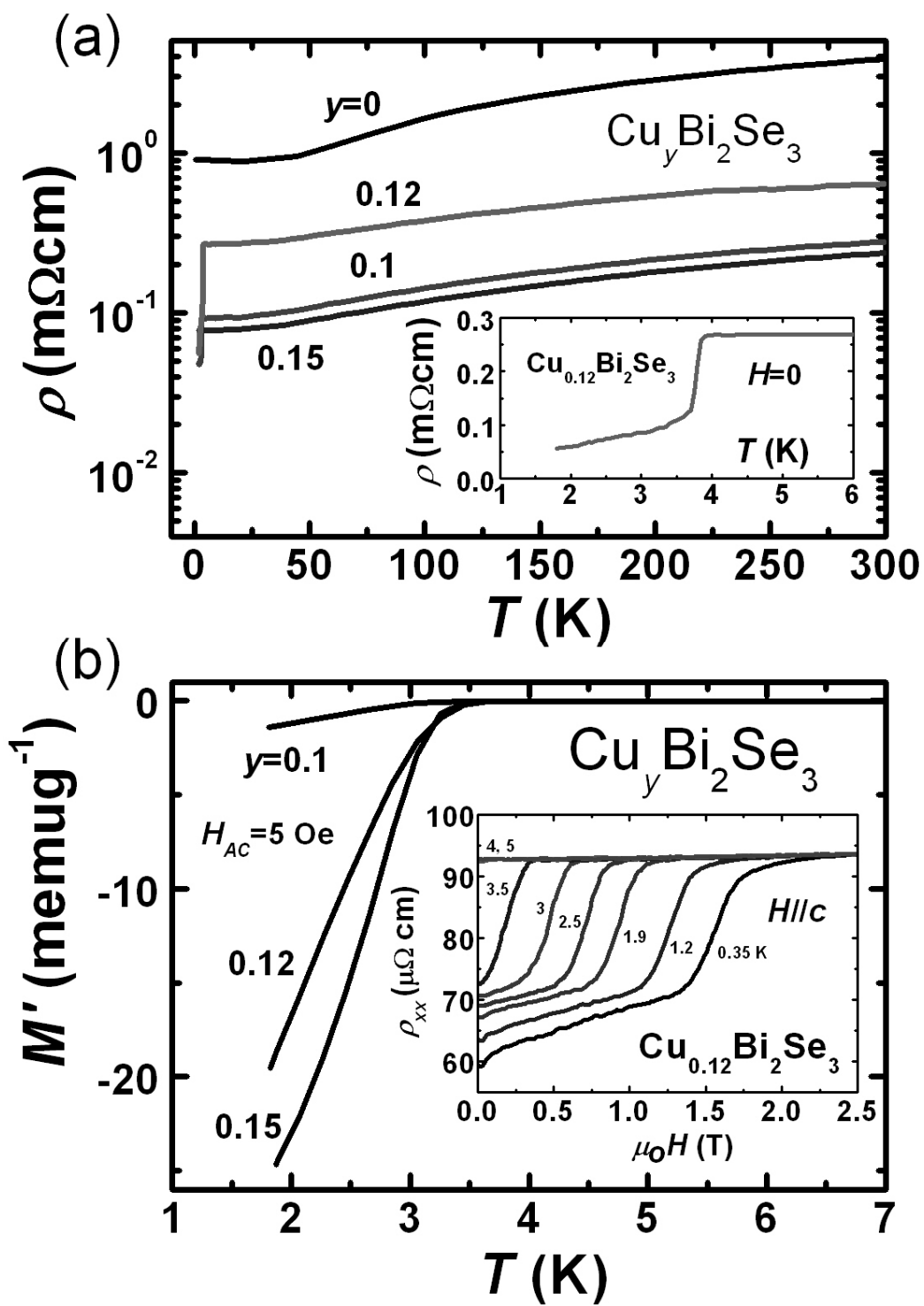


Figure 2

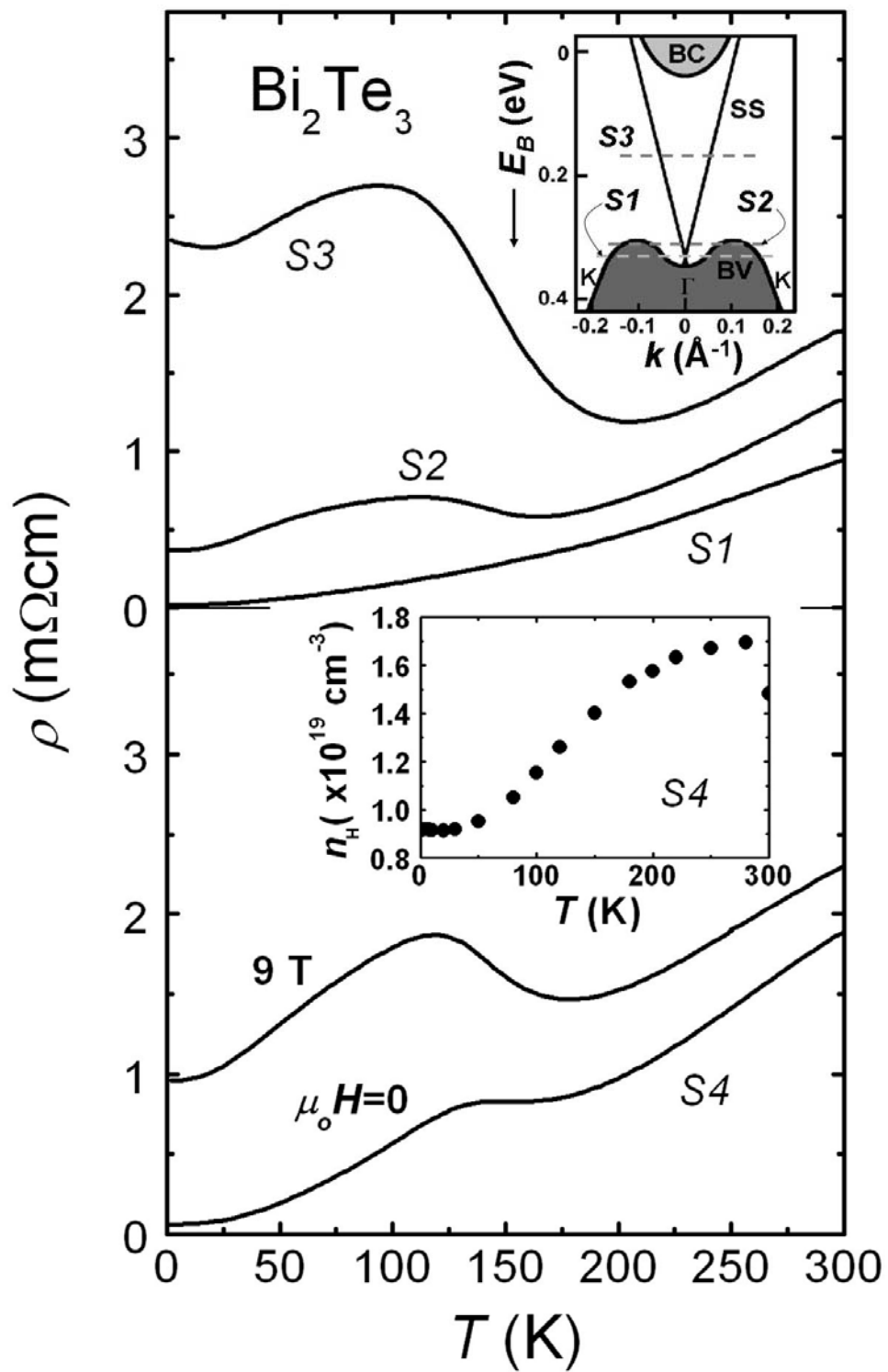


Figure 3

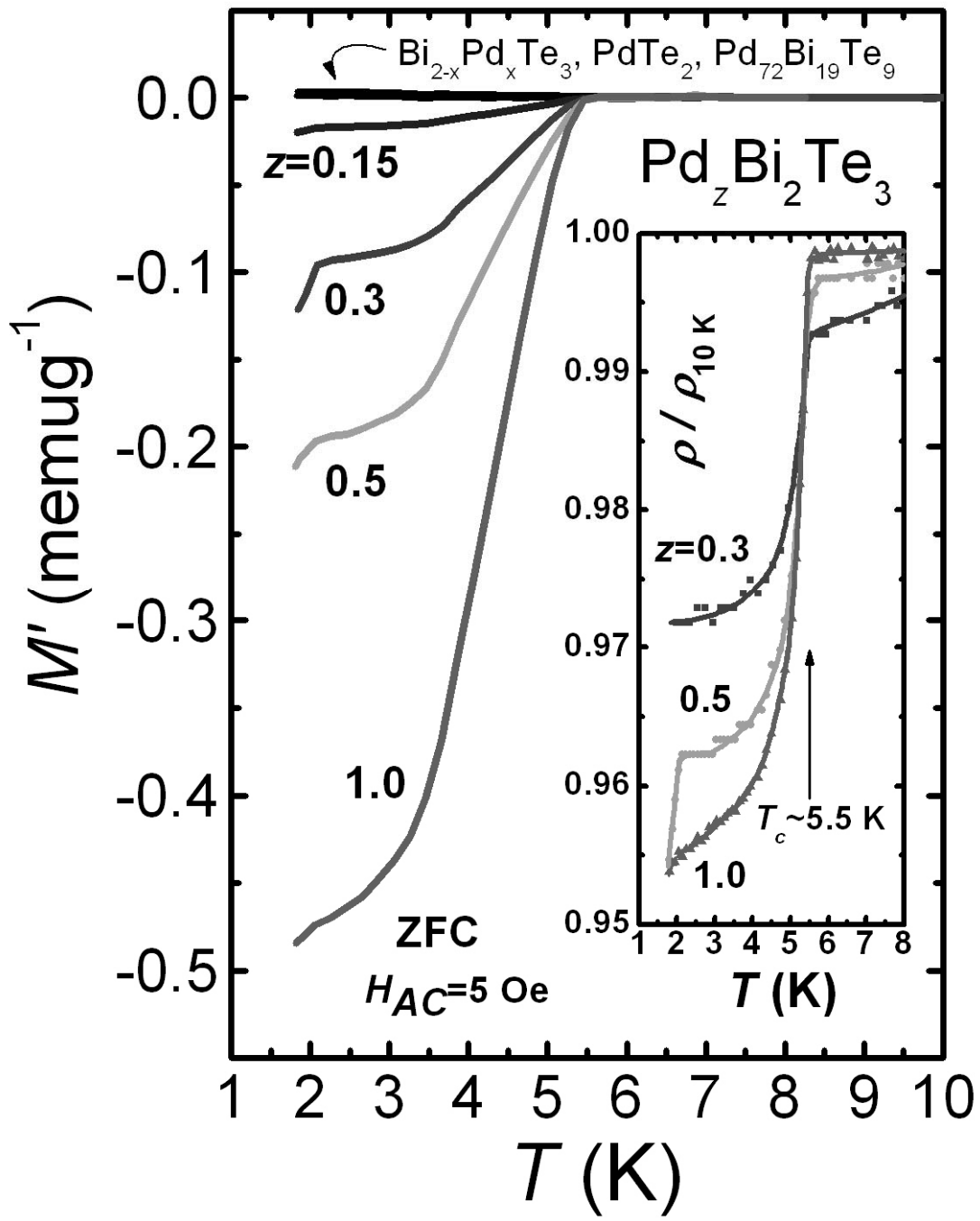


Figure 4